JOURNAL OF GEOPHYSICAL RESEARCH, VOL. 88, NO. B6, PAGES 4984–4996, JUNE 10, 1983

A Dislocation Model of Strain Accumulation and Release at a Subduction Zone

J. C. SAVAGE

U.S. Geological Survey, Menlo Park, California 94025

Strain accumulation and release at a subduction zone are attributed to stick slip on the main thrust zone and steady aseismic slip on the remainder of the plate interface. This process can be described as a superposition of steady state subduction and a repetitive cycle of slip on the main thrust zone, consisting of steady normal slip at the plate convergence rate plus occasional thrust events that recover the accumulated normal slip. Because steady state subduction does not contribute to the deformation at the free surface, deformation observed there is completely equivalent to that produced by the slip cycle alone. The response to that slip is simply the response of a particular earth model to embedded dislocations. For a purely elastic earth model, the deformation cycle consists of a coseismic offset followed by a linear-in-time recovery to the initial value during the interval between earthquakes. For an elastic-viscoelastic earth model (elastic lithosphere over a viscoelastic asthenosphere), the postearthquake recovery is not linear in time. Records of local uplift as a function of time indicate that the long-term postseismic recovery is approximately linear, suggesting that elastic earth models are adequate to describe the deformation cycle. However, the deformation predicted for a simple elastic halfspace earth model does not reproduce the deformation observed along the subduction zones in Japan at all well if stick slip is restricted to the main thrust zone. As recognized earlier by Shimazaki, Seno, and Kato, the uplift profiles could be explained if stick slip were postulated to extend along the plate interface beyond the main thrust zone to a depth of perhaps 100 km, but independent evidence suggests that stick slip at such depths is unlikely.

INTRODUCTION

As is well known, a simple screw dislocation model [*Savage and Burford*, 1973] yields a rough quantitative description of the strain accumulation and release process along transform faults. There does not appear to be a similar edge dislocation model to describe the subduction process. This paper describes a simple two-dimensional model designed to represent strain accumulation and release associated with the great, shallow, thrust earthquakes that occur at subduction zones. The solutions for strain accumulation and surface deformation are taken directly from dislocation theory and, in the case of the least complex earth model are similar to the finite-element model [*Shimazaki*, 1974*a*] used to describe subduction off the coast of Japan. However, the present model is free from the arbitrary constraints imposed on the finite element model and is easily generalized to more complicated models. In particular, the dislocation model is quite compatible with computational schemes [*Rundle*, 1978, 1982] developed for the calculation of deformation in an elastic-viscoelastic earth model (an elastic lithosphere over a viscoelastic asthenosphere). Coseismic and short- term postseismic phenomena in the elastic-viscoelastic earth model are the same as described by *Thatcher and Rundle* [1979]. The new factor in this model is the inclusion of a different representation of the strain accumulation process. Finally, evidence is cited that suggests that the viscoelastic response of the asthenosphere is not of overwhelming importance, and, consequently, a simple elastic earth model may be an adequate basis for approximating the deformation during the earthquake cycle.

Davies and House [1979] have described a typical subduction zone as follows: The interface between the subducted and overriding plates dips gently (10°-15°) landward from its surface trace at the oceanic trench to a depth of about 40 km. The interface then bends rather sharply to attain a dip of 30° or more as the subducted plate plunges into the asthenosphere. The shallow, gently dipping section of the interface is called the main thrust zone, whereas the more steeply dipping portion of the interface (the upper boundary of the Benioff zone) will be called the Benioff interface. The general configuration is shown in Figure 1. Precise hypocentral locations and focal mechanism solutions for earthquakes in subduction zones [*Yoshii*, 1979; *Davies and House*, 1979] indicate that along the main thrust zone the predominant mechanism is thrusting on the surface of the zone, whereas the activity in the Benioff zone is neither concentrated on the Benioff interface nor is it consistent with slip parallel to the interface. These observations are summarized by the statement that interplate earthquakes occur on the main thrust zone but intraplate events occur in the Benioff zone. It is inferred that interplate motion is accommodated by stick slip on the main thrust zone but by continuous aseismic slip on, or distributed shear across, the Benioff interface. This model of subduction is similar to the conventional model of a transform fault [*Savage and Burford*, 1973] in which the fault slips aseismically at depth but closer to the surface remains locked except during occasional catastrophic slip events.

In the dislocation model I will require that the main thrust zone act as a unit, exhibiting no slip in the interval between great earthquakes and slipping uniformly at the time of a great earthquake. *Kawakatsu and Seno* [1983] have shown that in some sections along the Japanese coast the main thrust zone is composed of two segments: a shallow thrust zone (depth 0-40 km) and a deep thrust zone (depth 40-60 km). The two segments may rupture independently, the shallow zone being the source of great earthquakes ($M \sim 8.0$), whereas the deep segment is the source of large ($M \sim 7.4$) earthquakes. Neighboring sections apparently do not exhibit this behavior. Moreover, the actual rupture areas mapped for various great earthquakes off the coast of Japan [*Kawakatsu and Seno*, 1983] suggest that the locked areas may consist of isolated patches on a continuously slipping main thrust

Paper number 3B0338.

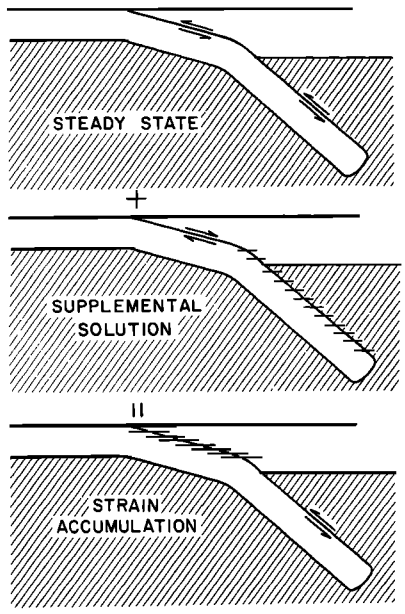

Fig. 1. Superposition model of strain accumulation at a subduction zone. The asthenosphere is indicated by shading. A locked (no slip) condition at an interface is indicated by short horizontal bars crossing the interface.

zone. These possibilities are not considered in the simple dislocation model proposed here.

DISLOCATION MODEL

The model of strain accumulation and release at a subduction zone considered here is simply a perturbation of steady state subduction. In steady state subduction the subducted plate slides uniformly along its length downward into the asthenosphere at the plate convergence rate. Steady state subduction is the long-term average motion that occurs at seismic subduction zones and may be the actual process that occurs at aseismic subduction zones (e.g., Mariana Islands). Clearly, steady state subduction involves uniform reverse slip at the plate convergence rate on the main thrust zone and presumbaly upon the upper part of the Benioff interface. At greater depths, discrete slip on the interface must grade into distributed shear across a boundary layer in the asthenosphere. Strain accumulation is generated in this model by locking (i.e., imposing a no-slip condition upon) the main thrust zone. This locking is represented simply by adding a supplemental solution that imposes normal slip at the plate convergence rate upon the main thrust zone. The superposition is shown schematically in Figure 1. Obviously, both steady state subduction and the supplemental process must be linear in order to obtain a valid solution by superposition. Thus the scheme in Figure 1 would not apply to models in which the flow in the asthenosphere is nonlinear. In addition to steady normal slip at the plate convergence rate, the supplemental solution must provide occasional abrupt thrust events to recover the accumulated normal slip. These abrupt thrust events, of course, represent the major, shallow, thrust earthquakes that occur at the subduction zone. The superposition of the supplemental and steady state solutions then gives a complete representation of the earthquake cycle.

In steady state subduction the movement of the lithospheric plates is specified by the kinematic description: The subducted plate slips steadily along its own length into the asthenosphere at the plate convergence rate. Complex motions in the asthenosphere are required to accommodate the lithosphere subduction, but those motions are not involved in the calculation of the deformation at the free surface. Thus the kinematic description suffices for our purposes, and it seems most likely that in steady state subduction neither appreciable strain nor deformation accumulates at the free surface of the overthrust plate. (The alternative would imply enormous cumulative deformation over the millions of years during which subduction has occurred. Although large amounts of deformation are evident within the accretionary wedge, similar amounts are not evident in the overthrust plate proper [see, e.g., *Abe*, 1978, p. 264; *Seno*, 1979, p. 44]). Because it is only at the free surface of the overthrust plate that strain and deformation can be measured, the steady state solution should not contribute to the observable changes.

The supplemental solution is simply the response of the earth model to the repeated imposition of a slip cycle on the main thrust zone. The cycle consists of a long interval of normal slip at the plate convergence rate followed by an abrupt thrust event that recovers the accumulated slip. This is not to say that normal slip actually occurs on the main thrust zone. On the contrary, the normal slip from the supplemental solution is cancelled by the reverse slip from the steady state subduction solution so that a no-slip condition obtains on the main thrust zone except at the time of the abrupt thrust events in the supplemental solution. Nevertheless, because the steady state subduction solution does not contribute to strain or deformation changes on the surface of the overthrust plate, the deformation there during the strain accumulation phase is indistinguishable from that produced by normal slip on the main thrust zone. Thus normal slip on the main thrust zone is equivalent to the actual strain accumulation mechanism. This result was apparently recognized by *Yamashina* [1976] much earlier.

The supplemental solution is easily generalized to the case of oblique subduction by including strike slip on the main thrust zone. The steady state subduction solution then involves a transverse motion parallel to the plate boundary in addition to the convergence previously discussed. The supplemental solution will include, in addition to the dip slip motions already described, a backward (i.e., opposite sense from the relative transverse plate motion) stike slip component of imposed slip on the main thrust zone at the rate of relative transverse plate motion. Morever, the occasional catastrophic slip events in the supplemental solution must include a forward strike slip component that recovers the slowly accumulated, backward, lateral slip at the same time as the slowly accumulated, normal, dip slip is recovered.

The solution to the supplemental problem (i.e., deformation induced by slip on the main thrust zone) is a straightforward application of dislocation theory: An edge dislocation located at the downdip edge of the main thrust zone with its Burgers vector parallel to the zone reproduces the effects of dip slip faulting, and a congruent screw dislocation reproduces the effects of strike slip faulting. The magnitude of the Burgers vector must vary as a sawtooth function of time, increasing gradually at the plate convergence rate during the interseismic period and decreasing abruptly to zero at the time of the earthquake. Thus all that is required for the supplemental solution is a knowledge of the response of a realistic earth model to embedded edge and screw dislocations. To the extent that the earth can be represented by an elastic half space, the solutions are well known. They become more complicated as allowance is made for the actual complex heterogeneous elastic structure of the earth in the vicinity of a subduction zone. A more important consideration involves mak-

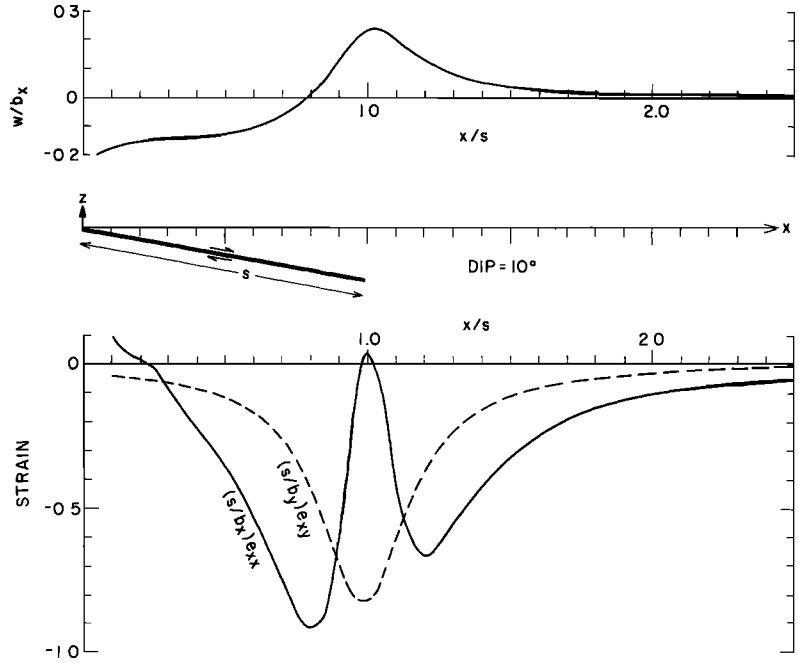

Fig. 2. The elastic half-space, dislocation model of strain accumulation at a subduction zone. The middle diagram shows a vertical cross section with the main thrust zone dipping 10°. The upper figure shows the vertical uplift generated by normal slip of amount b_x on the main thrust zone, and the lower figure shows the strains generated by normal slip b_x and transverse slip b_y on the main thrust zone.

ing some provision to represent the time-dependent response of the asthenosphere. The elastic-viscoelastic earth model (an elastic plate over a viscoelastic half space) is the least complicated model that allows for asthenosphere relaxation. Finally, the representation of fault slip by discrete (Volterra) dislocations requires uniform slip over the entire main thrust zone. A more sophisticated model might require that the dislocations be smeared out somewhat so that the termination of slip at the downdip end of the main thrust zone is not so abrupt.

Elastic Half-Space Earth Model

The solution of the supplemental problem requires the specification of an appropriate earth model, and in this section the simplest such model, an elastic half space, is considered. A right-handed coordinate system is employed with the y axis along the surface trace of the main thrust zone, the x axis horizontal and directed along the dip azimuth of the main thrust zone, and the z axis directed vertically upward. A mixed dislocation parallel to the y axis with its Burgers vector in the plane of the main thrust zone is located at the downdip end of the main thrust zone. The use of a line dislocation (i.e., infinite length) implies that subduction is uniform along strike for a large distance so that the problem is two dimensional. The surface deformation can be described by three components: A uniaxial strain e_{xx} and vertical displacement w produced by the edge dislocation component of the mixed disclocation and a simple shear e_{xy} parallel to the y axis produced by the screw dislocation component. The third component of surface strain e_{yy} (extension parallel to the strike of the main thrust zone) is taken to be zero in this two-dimensional model. Expressions for the three components of deformation are [*Mura*, 1968; *Freund and Barnett*, 1976]:

$$e_{xx}=(2b_x/\pi)\, s \sin\alpha\, (s-x\cos\alpha)\,(x-s\cos\alpha)/D^4 \quad (1)$$

$$w = (b_x \sin\alpha/\pi)\quad \{(xs\sin\alpha)/D^2 + \tan^{-1}[(x-s\cos\alpha)/(s\sin\alpha)]-\pi/2\}\quad x>0 \quad (2)$$

$$e_{xy} = (b_y\, s \sin\alpha)/(2\pi D^2) \quad (3)$$

where

$$D^2=x^2 + s^2 - 2xs\cos\alpha \quad (4)$$

x is the distance of the observer from the surface trace of the main thrust zone, s is the downdip width of the main thrust zone, α is its dip, and b_x and b_y are the dip slip and strike slip components (normal and right-lateral slip taken as positive) of the Burgers vector. The three components of deformation are plotted in Figures 2 and 3 for dips of the main thrust zone equal to 10° and 30°, respectively. The Burgers vectors b_x and b_y in (1), (2), and (3) are sawtooth functions of time with the slope of the ramp equal to the perpendicular plate convergence rate (B_x) for b_x and to the transverse component of relative plate velocity (B_y) for b_y. The duration of the ramp is simply the earthquake interoccurrence time T. Thus

$$b_i = B_i\,(t - nT)\quad nT< t< (n+1)T \quad (5)$$

where n is an integer specifying the sequence number of the earthquake and t is the time measured from the earthquake identified by $n=0$.

The supplemental solution is best discussed by reference to the shallow dip solution shown in Figure 2. Because in this discus-

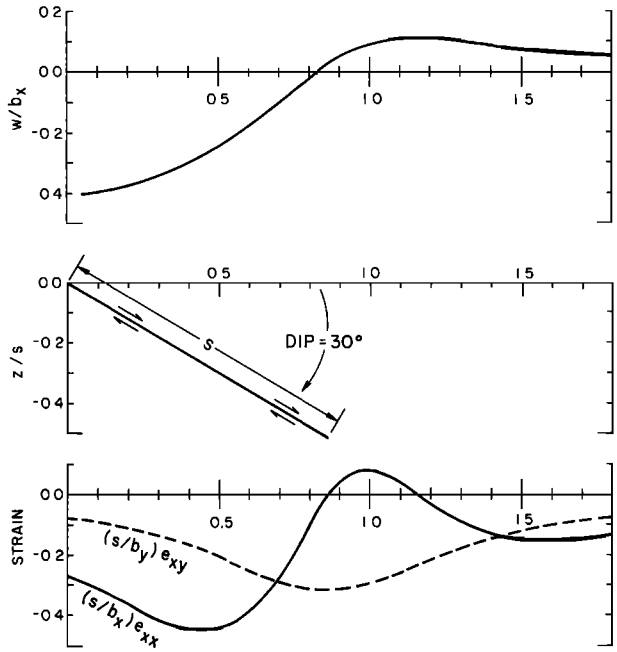

Fig. 3. Same as Figure 2 except main thrust zone dip is 30°.

sion we will be concerned with the strain accumulation cycle, b_x will be positive. Inasmuch as typical values of s (downdip width of the main thrust zone) are not less than about 100 km and plate convergence rates do not much exceed 100 mm/a, maximum strain rates should be less than 1.0 microstrain/a and the uplift rates should be less than 25 mm/a during the strain accumulation cycle.

A curious feature of the e_{xx} component of strain in Figure 2 is the anomalous strain in the interval $s \cos \alpha < x < s/\cos \alpha$. Everywhere else the strain is less than zero, indicating compression as expected during the strain accumulation cycle, but in that small interval tensile strain occurs. Presumably, this reversal in strain is related to the longitudinal strain induced by flexure at the free surface (Figure 2). However, the strain anomaly depends rather critically upon the discrete-dislocation representation used in the supplemental solution. If the termination of slip at the downdip end of the main thrust zone were less abrupt, the strain curves in Figure 2 would be smoothed at the expense of the extreme values (Figure 4). To the extent that the discrete-dislocation representation is appropriate, the strain field above the downdip end of the main thrust zone in oblique subduction may be dominated by transverse shear (e_{xy}) rather than compression normal to the plate boundary (Figures 2 and 3).

From (2) it is easily shown that the maximum uplift occurs at $x = s/\cos \alpha$ and is equal to

$$w_{max} = (b_x/\pi)[\cos \alpha + (\alpha - \pi/2) \sin \alpha] \quad (6)$$

The maximum uplift is a decreasing function of α. For $x < s/\cos \alpha$, tilting is toward the sea, and for $x > s/\cos \alpha$, tilting is toward the land. For dips between 10° and 30°, $w(x,t)$ changes sign quite close to $x = 0.8$ s; uplift occurs on the landward side of $x = 0.8$ s and subsidence on the seaward side. These critical values of x (0.8 s and $s/\cos \alpha$) are useful in fitting a dislocation model to an observed uplift profile.

Equations (1), (2), and (3) can easily be generalized to include more complicated fault geometries than shown in Figures 2 and 3. For example, the case of normal slip confined to a buried segment of a fault will be required later. Clearly, that solution can be generated by superposing two dislocation solutions, one representing reverse slip from the surface to the top of the buried fault segment and the other representing normal slip from the surface to the bottom of the buried fault. Furthermore, the effects of dip slip on a curved fault can be represented by approximating the curved surface by a sequence of planar buried fault segments, each with a slightly different dip. Such an approximation is not necessary for strike slip on a curved surface as (3) is correct for any slip surface containing the dislocation.

ELASTIC-VISCOELASTIC EARTH MODEL

The elastic-viscoelastic earth model, consisting of an elastic plate (lithosphere) overlying a viscoelastic half space (asthenosphere), makes some allowance for flow in the asthenosphere and, consequently, is a more realistic representation of the earth than the simple elastic half-space model. Appropriate solutions for dislocations in the elastic-viscoelastic earth model have been discussed by *Rundle* [1978] and *Thatcher and Rundle* [1979] for edge dislocations and by *Nur and Mavko* [1974] for screw dislocations. Indeed, *Thatcher and Rundle* [1979] have discussed the complete dip slip earthquake cycle in an elastic-viscoelastic earth model based on a strain accumulation mechanism differing from that employed here. They postulated that steady buried, reverse slip on the plate interface in the lower lithosphere approximates the effects of plate convergence, whereas in this paper, steady normal slip on the main thrust zone is shown to be equivalent to plate convergence. The two mechanisms are similar but not equivalent.

The supplemental solution for an elastic-viscoelastic earth model can be written as the sum of the contributions from the strain accumulation mechanism (equivalent to normal slip on the main thrust zone) and the contributions from the individual thrust earthquakes including postseismic effects. Consider a long period

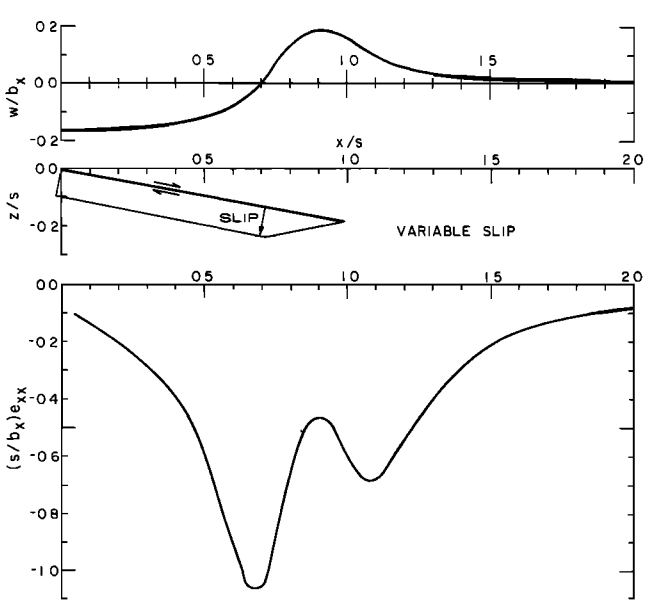

Fig. 4. Same as Figure 2 except that the normal slip is not constant over the entire breadth of the main thrust zone but rather tapers linearly to zero from its value of b_x maintained over the shallowest 4/5 of the fault, as indicated by the shading adjacent to the main thrust zone.

of time during which strain accumulation has gone on steadily and thrust events have occurred regularly with periodicity T. Let $w(x,t)$ represent one component of deformation (e.g., uplift) measured at time t and at a distance x from the oceanic trench, and let $w_N(x,t)$ represent the contribution of the strain accumulation mechanism (equivalent to normal slip on the main thrust zone) to the total response $w(x,t)$. Finally, let $w_1(x,t)$ be the response of the elastic-viscoelastic earth model to a single isolated thrust event occurring at time $t = 0$ on the main thrust zone. Then, for $0 < t < T$,

$$w(x,t) = w_N(x,t) + w_1(x,t) + \sum_{n=1}^{\infty} w_1(x,t+nT) \quad (7)$$

where t is measured from just prior to the most recent earthquake. Because $w_N(x,t)$ is the response to a steady motion of long duration, it must itself be a steady motion of the form $\gamma(x)t + c(x)$. Moreover, measurement of deformation must always be referred to an arbitrary reference configuration, taken here to be the configuration at $t=0$. Then substituting $\gamma(x)\,t + c(x)$ for $w_N(x,t)$ in (7) and evaluating $c(x)$ by requiring $w(x,0) = 0$, we have

$$w(x,t) = \gamma(x)\,t + w_1(x,t) + \sum_{n=1}^{\infty} [w_1(x,t+nT) - w_1(x,nT)] \quad (8)$$

Because there is no secular accumulation of deformation in the dislocation model, $w(x,t)$ must be periodic function of t with period T. Therefore

$$w(x,T) = w(x,O) = 0$$

and evaluating (8) at $t=$T (at which time adjacent terms in the series cancel identically) requires

$$\gamma(x) = -w_1(x,\infty)/T \quad (9)$$

Thus the supplemental solution for the elastic-viscoelastic earth model can be expressed in terms of the response function of that model to an individual thrust event:

$$w(x,t) = -w_1(x,\infty)\,t/T + w_1(x,t) + \sum_{n=1}^{\infty} [w_1(x,t+nT) - w_1(x,nT)] \quad 0<t<T \quad (10)$$

Rundle [1978] and *Thatcher and Rundle* [1979] have shown how to calculate the function $w_1(x,t)$ for dip slip faulting, and several examples of the surface uplift produced by a single thrust earthquake in an elastic-viscoelastic model have been calculated by *Thatcher and Rundle* [1979] and *Thatcher et al.* [1980]. In those examples the viscoelasticity in the asthenosphere has been represented by a Maxwell solid. The coseismic response is, of course, the same as in the elastic model, and the postseismic response in the region $0.5< x/s <1.5$ is a subsidence centered over the downdip end of the main thrust zone (Figure 5). This subsidence maintains its general shape but increases in amplitude as time increases, approaching a limiting profile [*Thatcher and Rundle*, 1979]. The limiting profile $w_1(x,\infty)$ is simply the relaxed response of the elastic-viscoelastic model (i.e., the response of an elastic earth model formed by replacing the complex moduli in the viscoelastic half space by their relaxed equivalents). Notice that this same limiting value determines the response of the elastic-viscoelastic model to the strain accumulation mechanism (9).

Given the function $w_1(x,t)$, one can construct the response to the earthquake cycle from (10). That response can be divided into two parts, the first term in (10) being the response to the strain accumulation mechanism and the second and third terms simply the response to the earthquake sequence.

Consider the earthquake response (shown schematically by the dash-dot line in Figure 6) first. Starting from zero deformation at $t=0$, the deformation immediately jumps discontinuously to $w_1(x,0^+)$ with the occurrence of the earthquake. Then relaxation of stresses imposed on the viscoelastic half space by that earthquake and its predecessors causes a gradual postseismic deformation reaching $w_1(x,\infty)$ at $t=T$. The net deformation $w_1(x,\infty)$ attained at $t=$T is exactly that which would be attained in infinite time after a single earthquake. The magnitude of $w_1(x,\infty)$ may be either greater or less than the magnitude of $w_1(x,0^+)$ depending upon whether the asthenosphere relaxation increases or decreases the particular component of deformation. The uplift sketched in Figure 6 is that expected for $0.9 < x/s < 1.5$ (Figure 5).

The competing component of deformation is that due to the strain accumulation mechanism (equivalent to normal slip on the main thrust zone). That mechanism produces a steady rate of accumulation of deformation shown schematically by a dashed line in Figure 6 such that $-w_1(x,\infty)$ is attained in the interseismic period T.

The actual deformation (shown schematically by a solid line in Figure 6) is the sum of the strain accumulation response and the earthquake response. The discontinuous coseismic response dominates the sum at $t=0^+$, but subsequently, the strain accumulation response tends to overcome the earthquake response, reducing the deformation to zero at $t=T$.

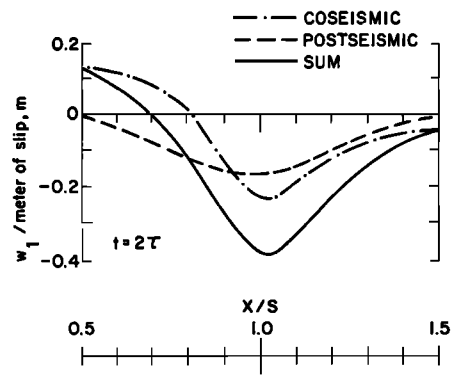

Fig. 5. Uplift produced by 1 m of reverse slip on the main thrust zone (downdip width s and dip 10°) in an elastic-viscoelastic model (elastic plate of thickness $H = s/3$ overlying a Maxwell solid half space). The postseismic uplift curve, taken from Figure 2 of *Thatcher et al.* [1980], represents deformation at $t = 2\,\tau_o$, where τ_o, is the characteristic relaxation time of the asthenosphere.

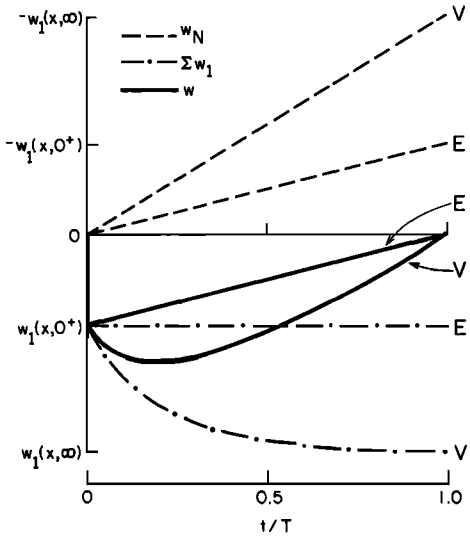

Fig. 6. Schematic diagram of deformation as a function of time for the elastic (*E*) and elastic-viscoelastic (*V*) earth models. The solid lines represent the net deformation, the dashed lines represent the contributions from the strain accumulation mechanism, and the dash-dot lines represent the coseismic plus postseismic contributions. The time axis extends from just prior to one earthquake to just prior to the succeeding one.

A schematic comparison of the responses of an elastic-viscoelastic model and an elastic model to a periodic sequence of thrust earthquakes is shown in Figure 6. To facilitate comparison of the two models, the elastic-viscoelastic model is restricted to the case in which the unrelaxed moduli of the viscoelastic half space are equal to the elastic moduli of the overlying layer. The coseismic response in the two models is then the same. In the diagram $|w_1(x,\infty)| > |w_1(x,0)|$, but that need not be the case. The elastic and elastic-viscoelastic models differ in their recovery from the coseismic offset; the elastic model recovers linearly, whereas the elastic-viscoelastic model recovers at a variable rate. Because the elastic and elastic-viscoelastic responses are identical for $t=0^+$ and $t=T$, it is likely that the two models will give similar measures of the change in deformation over a time interval that is comparable to the interseismic period T (see Figure 6). Although this is a rather inexact specification, it may be useful where deformation is inferred from a comparison of recent geodetic surveys with those made at the turn of the century.

A detailed discussion of the earthquake cycle for perpendicular plate convergence in an elastic-viscoelastic earth model employing the strain accumulation mechanism described in this paper has been undertaken by *Thatcher and Rundle* [1981]. In their model the asthenosphere is represented by a Maxwell solid. The reader is referred to their work for further details on deformation in the elastic-viscoelastic earth model.

The supplemental solution for the transverse component of relative plate motion in an elastic-viscoelastic model is appreciably simpler than for the normal component of relative plate motion, and solutions have been given by *Savage and Prescott* [1978] and *Spence and Turcotte* [1979]. Both solutions are restricted to the case where the viscoelastic half space behaves as a Maxwell solid, and the Spence-Turcotte solution requires the downdip end of the main thrust zone to lie on the lithosphere-asthenosphere boundary. The required strain (e_{xy}) solution is shown directly by *Spence and Turcotte* [1979, Figure 6], whereas it must be deduced from the slope of the displacement-versus-distance plots of *Savage and Prescott* [1978]. One example given by *Spence and Turcotte* [1979] is reproduced in Figure 7. The critical distance parameter in that plot is the distance from the line on the surface directly above the downdip edge of the main thrust zone. Close to that line the strain rate decreases monotonically with time after the most recent earthquake, but at more distant points the strain rate may undergo a reversal in sign as time increases.

A comparison of the responses of an elastic model and an elastic-viscoelastic model to the transverse component of plate motion when accommodated by a periodic sequence of strike slip events on the main thrust zone is shown in Figure 7. In that comparison the main thrust zone cuts completely through the lithosphere, implying a maximum involvement of the asthenosphere. Better agreement between the elastic and elastic-viscoelastic models would be expected if the main thrust zone terminated within the lithosphere. The agreement between the two models depends upon the ratio T/τ_0, where T is the earthquake interoccurrence time and τ_0 is the asthenosphere relaxation time. (The latter quantity is defined as used by *Savage and Prescott* [1978] and *Thatcher and Rundle* [1979]; it is twice the relaxation time used by *Spence and Turcotte* [1979].) For $T/\tau_0<1$ the strains generated by the elastic and elastic-viscoelastic models are very similar [*Spence and Turcotte*, 1979, Figure 6*a*], but for $T/\tau_0 = 5$ (Figure 7) discrepancies as large as a factor 2 have developed. The usual estimates [*Thatcher and Rundle*, 1979, 1981; *Thatcher et al.*, 1980] of τ_0 fall in the range of 1 to 100 a (asthenosphere viscosities of 10^{19} to 10^{20} P), and a typical earthquake interoccurrence time T is 100 a. Thus the ratio T/τ_0 is likely to be about 10, and it would appear that the elastic-viscoelastic model would be required.

THE "DRAG" MODEL OF STRAIN ACCUMULATION

Shimazaki [1974*a*] proposed a 'drag' model (Figure 8) of deformation of the overthrust block at a subduction zone that is quite similar to the dislocation model in an elastic half space. In Figure 8 the horizontal surface represents the free surface of the overthrust block, and the surface sloping downward to the right represents the plate interface (main thrust zone plus the Benioff interface). The remaining surfaces (vertical surface on the right and the short segment sloping downward to the left) are assumed to be sufficiently remote (650 km or more in the model) from the oceanic trench as to be undisturbed by the earthquake cycle. Tangential displacements (indicated by arrows in the figure) are prescribed over the short interval of the plate interface supposed

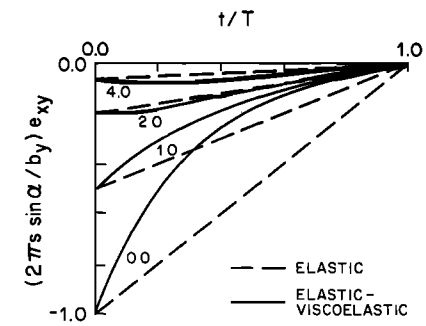

Fig. 7. Surface shear strain generated by transverse plate motion during the earthquake cycle in elastic (dashed lines) and elastic-viscoelastic (solid lines) earth models in which the main thrust zone cuts the entire lithosphere [from *Spence and Turcotte*, 1979, Figure 6b]. The interval between earthquakes is taken to be five asthenosphere relaxation times for the elastic-viscoelastic model. The curves are labeled by distance in units of lithosphere thickness ($s \sin \alpha$) from the point directly above the downdip end of the main thrust zone.

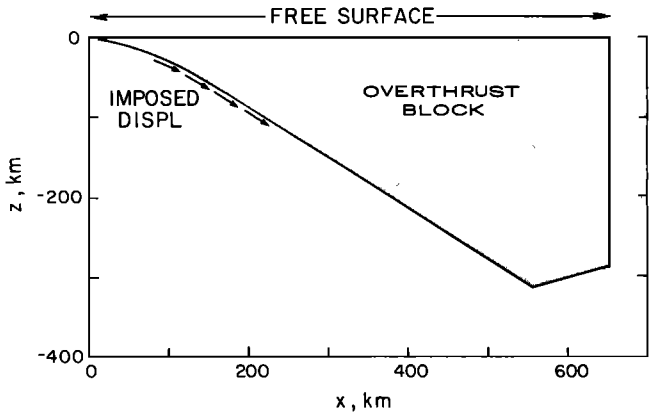

Fig. 8. Shimazaki's model of strain accumulation at a subduction zone. The shaded portion represents the overthrust block with the edge sloping downward to the right representing the interface between the overthrust and underthrust block. The upper horizontal surface is assumed to be stress free. Tangential displacements are imposed on the segment of the interface indicated by short arrows. The remainder of the boundary of the overthrust block is held fixed.

to be locked to the subducted plate. These imposed displacements represent the dragging effect of the subducted plate on the overthrust plate. The two plates are assumed to be decoupled over the remainder of the interface both above and below the locked section so that no drag is exerted there. Shimazaki has approximated this decoupling by imposing a no-displacement boundary condition. The deformation was then determined by finite element techniques. *Shimazaki* [1974*a*] found that the vertical deformation observed along the southeast coast of Hokkaido, Japan, could be approximated reasonably well (Figure 9) by imposing a uniform tangential velocity of 27 mm/yr along the plate interface in the depth interval 22-100 km. The perpendicular plate convergence rate along that coast is about 80 mm/yr, roughly 3 times greater than the imposed tangential velocity. *Seno* [1979] used the drag model to explain vertical deformation observed in a profile across Tohoku (northern Honshu), Japan. He found that a satisfactory fit could be obtained if a tangential velocity 35 mm/a were applied along the plate interface in the depth interval 22-100 km. The perpendicular convergence rate along the east coast of Tohoku is about 100 mm/a, again 3 times greater than the imposed tangential velocity. *Kato* [1979], citing arguments advanced earlier by Yoshii, noted that tight coupling between the two plates probably could not be maintained at depths greater than about 70 km and, consequently, tangential displacements should not be imposed at those depths. He suggested that vertical displacements might be appropriate at those depths, however, to represent cases where the subducted plate did not slip into the asthenosphere along its own length but rather sank somewhat more rapidly. *Scholz and Kato* [1978, p. 792] used the drag model to explain the deformation observed in south Kanto, Japan, but apparently they required the tangential displacements to be directed updip rather than downdip.

The drag model appears to be designed to approximate the same physical situation as the dislocation model described in this paper, namely, the case where steady state subduction is perturbed by imposing a no-slip condition on a shallow segment of the plate interface. The two models differ in that Shimazaki imposed displacement boundary conditions where only relative motion across the boundary (i.e., slip) was indicated. The dislocation techniques used in this paper are uniquely appropriate to the specification of relative motion across an interface. Thus the dislocation model is a better representation of the physical situation than is the drag model.

To determine the difference in deformation predicted by the dislocation model and the drag model, two dislocation models have been constructed that approximate slip on the curved section of the interface (along the arrows in Figure 8) upon which displacements were imposed by Shimazaki. The simple model consists of a buried planar segment dipping 30° that approximates the locked segment of the interface, and the more complex model consists of four contiguous planar segments of slightly differing dip that approximate the curvature of the locked segment somewhat better. The uplift and horizontal displacement profiles generated by 1.5 m of normal slip on those two dislocation models are compared in Figures 9 and 10 with similar profiles given by Shimazaki for his model *U* (1.5 m of drag on the locked section of the interface). The uplift profiles (Figure 9) for the two dislocation models are reasonably consistent, and both lie significantly above Shimazaki's uplift profile. It is not hard to see how this difference arises: Shimazaki's solution is arbitrarily constrained on

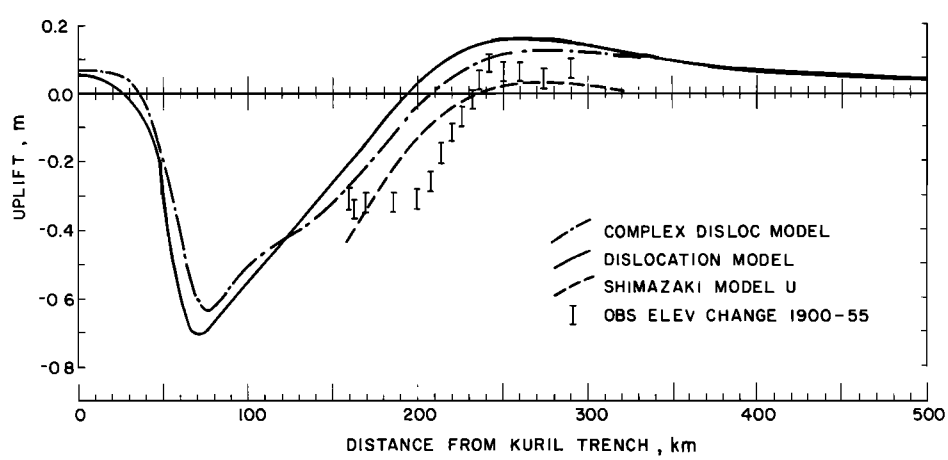

Fig. 9. A comparison of the uplift at the free surface caused by 1.5-m slip on the block interface in the depth interval 22-100 km as calculated by three different models. In the dislocation model the block interface is simply a plane dipping 30° embedded in an elastic half space. In the complex dislocation model the block interface is curved so as to more closely approximate the interface in the model in Figure 8. The Shimazaki solution and observed elevation changes 1903-1955 are taken from Figure 6 of *Shimazaki* [1974*a*].

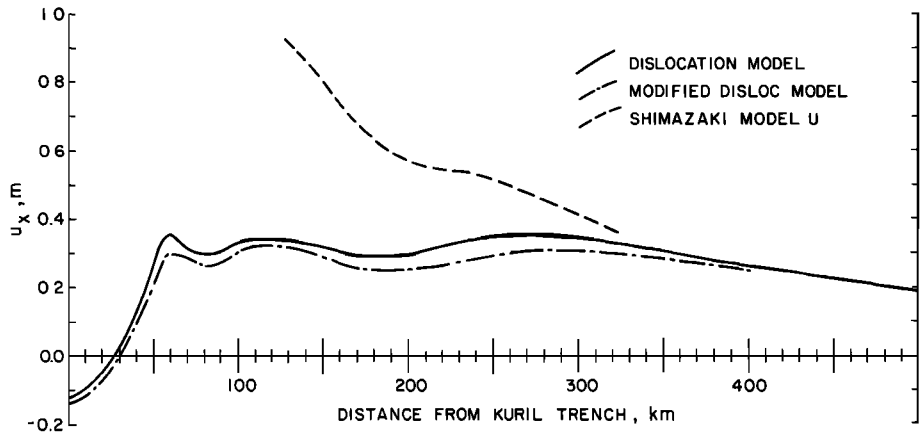

Fig. 10. Same as Figure 9 except that the horizontal displacement perpendicular to the strike of the subduction zone is shown and the curve for Shimazaki's model is taken from Figure 11 of *Shimazaki* [1974*a*].

the free surface to remain fixed at $x = 0$ and $x = 650$ km, whereas the unconstrained solution indicates an uplift at both points. Thus the arbitrary constraints distort the uplift by pulling the free surface downward. Also shown in Figure 9 is the 1903-1955 elevation change profile observed across southeastern Hokkaido [*Shimazaki*, 1974*a*]. The parameters in model *U* (1.5-m slip in depth interval 22-100 km) were chosen so that Shimazaki's model would approximate those observations. A minor modification of those parameters (principally extension of slip to greater depth) would bring the uplift profiles for the dislocation models more closely into coincidence with the observed profile.

The agreement between horizontal displacement profiles (Figure 10) calculated from the dislocation models on the one hand and from the drag model on the other is not as good as the uplift profiles. Indeed, the horizontal displacement profile given by Shimazaki appears tilted with respect to the dislocation model profile, indicating that the two solutions differ simply by an additive uniform strain $\partial u_x / x$ of about 2.7 microstrain in the interval $130 < x < 330$ km. This discrepancy is presumably due to the arbitrary no-displacement constraints imposed on the Shimazaki model.

The discrepancies between deformation predicted by the drag model and that predicted by the dislocation models shown in Figures 9 and 10 are not due to the more realistic distribution of elastic constants incorporated in the drag model. In fact, the discrepancies are increased when homogeneous elastic constants are substituted into the drag model (see the dotted curves in Figures 6 and 11 of *Shimazaki* [1974*a*]).

The differences between the 'drag' and dislocation models in Figures 9 and 10 are simply consequences of different input assumptions. The 'drag' model arbitrarily imposes boundary conditions upon the elastic wedge that represents the overthrust block, whereas the dislocation model assumes an elastic half-space earth model. Although neither prescription is correct, the dislocation model could be generalized to a more realistic earth model.

Approximate Elastic Earth Model

In comparing the deformation predicted by the dislocation model to the deformation actually observed, there appears to be justification for using elastic rather than elastic-viscoelastic earth models, at least near the downdip end of the main thrust zone. Specifically, the long-term postseismic recovery appears to be linear in time rather than displaying the variable rate expected where the viscoelastic effects are appreciable. For example, the change in elevation at Muroto Point on the south coast of Shikoku is shown as a function of time in Figure 11. Muroto Point apparently subsided at a uniform rate (7.5 mm/a) prior to the 1946 Nankaido earthquake, was uplifted more than 1 m at the time of the earthquake, subsided rapidly in the few years immediately after the earthquake, and then resumed a uniform subsidence at a rate (9.0 mm/a) very little different from the preseismic rate. The rapid postseismic subsidence (1946-1949) has been attributed to postseismic slip on the plate interface just beyond the coseismic rupture [*Thatcher and Rundle*, 1979], an effect not included in the dislocation model. If that effect is removed (or, perhaps better, included in the coseismic contribution), the remaining interseismic deformation is quite linear in time, as expected for an elastic model. Similarly, annual sea level measurements at Hanasaki on the southeast coast of Hokkaido indicate a uniform subsidence from 1910 to 1970 [*Abe*, 1978, p. 267]. The anomalous short-term (1894-1902) uplift immediately following the 1894 Kushiro-Oki earthquake has been attributed [*Shimazaki*, 1974*b*; *Kasahara*, 1975] to postseismic slip on the plate interface just beyond the coseismic rupture. Except for that immediate postseismic relaxation, the subsidence at Hanasaki is remarkably uniform in time. The record at Tohoku is ambiguous: *Kato* [1979, p. 1959] showed that the uplift rates in the 1894/1899-1942 inter-

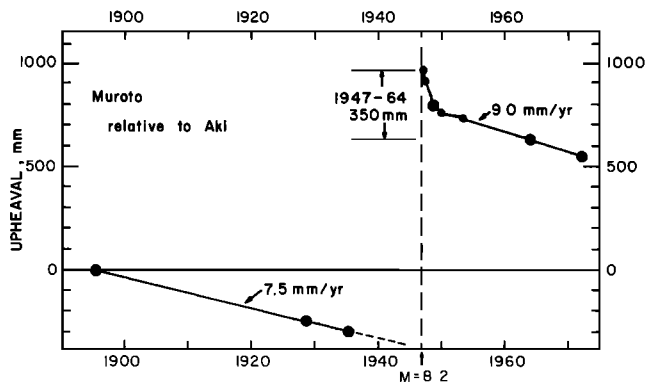

Fig. 11. Uplift of Muroto Point relative to Aki (40 km to the north-northwest) as determined by leveling surveys [*Thatcher and Rundle*, 1979]. Uplift inferred from partial surveys of the leveling route are represented by smaller plotted points. The discontinuous uplift in 1946 coincides with the Nankaido earthquake.

val differ from those in the subsequent interval (1942-1973). However, the difference there may be due to coseismic disturbances in 1897 and 1936 rather than to time-dependent, long-term postseismic recovery. *Wahr and Wyss* [1980, Figure 4] show several examples of postseismic recovery for Alaskan earthquakes, but the precision of measurement and the duration of the records are insufficient to determine whether the long-term recovery is linear in time. On the whole, convincing evidence for the strongly time-dependent, long-term postseismic recovery expected from asthenosphere relaxation is lacking in the available deformation records.

The absence of time-variable effects due to asthenosphere relaxation in the long-term response suggests that the asthenosphere relaxation time τ_0 must be quite short compared to the earthquake interoccurrence time T. In that case the earthquake response terms (Σw_1 in Figure 6) will rise quickly to an equilibrium value and then maintain that value. As a consequence, the time dependence of the net deformation will, except for a short postearthquake interval in which viscoelastic effects are important, be the linear-in-time response (W_N in Figure 6) due to the strain accumulation mechanism. As already pointed out this latter response is an elastic response in which the elasticity is governed by the relaxed elastic moduli for the asthenosphere. For a Maxwell solid, the usual representation of the asthenosphere, the relaxed rigidity is zero. Thus outside of the immediate postearthquake interval, an adequate earth model should be simply an elastic plate overlying a perfect fluid.

Rundle [1982] has shown that at least in the source area, the inclusion of gravity in the problem tends to confine viscoelastic relaxation to a short postseismic interval. This apparently arises because buoyancy forces tend to oppose further viscoelastic relaxation. Furthermore, the importance of asthenosphere relaxation is diminished as the lithosphere thickness H is increased in comparison to the depth h penetrated by the main thrust zone [*Thatcher et al.*, 1980, Figure 2] and further diminished if the asthenosphere is represented by a layer rather than a substrate [*Matsu'ura et al.*, 1981]. Thus it is not surprising that viscoelastic relaxation may be confined to the immediate postearthquake time interval in the source area, as suggested by Figure 11. It is likely, however, that viscoelastic relaxation effects may be of longer duration as one recedes from the source area. This is suggested by *Rundle*'s [1982, Figure 4] calculations.

The preceding arguments suggest that the proper model for the thrust strain accumulation cycle is simply an edge dislocation embedded in an elastic plate that overlies a fluid substrate. In fact, unless gravity is specifically taken into account, that solution is no different from the solution for a free elastic plate given by *Moss and Hoover* [1978]. However, *Rundle* [1982] has shown that the effects of gravity (more specifically buoyancy) are important in determining the solution for an elastic plate overlying a fluid substrate, and, in fact, that solution is given as the limiting case of Rundle's elastic-viscoelastic solution. We will not pursue this additional complication but rather confine ourselves to the elastic half-space solutions. We will, however, use Rundle's solution to evaluate qualitatively the changes that the more complete solution would impose. The comparable solution for transverse motion corresponds to a screw dislocation in an elastic plate and does not involve gravity. That solution has been given by *Nur and Mavko* [1974]. (See also a similar solution by *Turcotte and Spence* [1974].) However, there is little need for the elastic free-plate solution for the screw dislocation, as the complete elastic-viscoelastic solution is available (Figure 7).

COMPARISON WITH OBSERVED DEFORMATION

The deformation predicted by the dislocation model using an elastic half-space earth model can be compared to that observed along the coast of Japan. In this comparison, stick slip behavior is restricted to the main thrust zone. All model parameters are determined from independent data, and there are no arbitrary disposable constants to improve the fit. Off the coast of Japan the depth of the oceanic trench is about 6 km; the downdip end of the main thrust zone should lie at a depth of about 40 km [*Davies and House*, 1979], and the average width of the main thrust zone is about 200 km (see below). The dip of the main thrust zone is then about 10°, and the dislocation model conforms to that in Figure 2.

The observed deformation is derived from geodetic surveys in Shikoku, Tohoku (northern Honshu), and Hokkaido, Japan. The pertinent model parameters for each of these areas are as follows: The downdip edge of the main thrust zone is taken to coincide with the aseismic front in Tohoku and Hokkaido [*Yoshii*, 1979] and with the flexure of the subducted plate at 40-km depth in Shikoku [*Hirahara*, 1981, Figure 2]. The downdip width of the main thrust zone is then about 200 km. Off Shikoku the Philippine plate is subducted beneath the Eurasian plate at a rate of about 40 mm/a [*Seno*, 1977] in a direction approximately perpendicular to the plate boundary (Nankai trough). The Pacific plate is subducted beneath the Eurasian plate at a rate of about 100 mm/a. Off Tohoku the relative plate motion is approximately perpendicular to the plate boundary (Japan trench), but off Hokkaido the relative motion is oblique to the plate boundary (Kuril trench). The approximate annual values for b_x are 40, 100, and 80 mm and for b_y 0, 0, and 60 mm off Shikoku, Tohoku, and Hokkaido, respectively. Given these values of s, b_x, and b_y, one can estimate from Figure 2 the annual rates of strain accumulation and surface uplift that should be observed in Shikoku, Tohoku, and Hokkaido.

A comparison of the predicted and observed rates of uplift for Shikoku, Tohoku, and Hokkaido is shown in Figure 12. For Shikoku the observed uplift rates [*Thatcher and Rundle*, 1979] are based on changes in elevation between leveling surveys in 1895 and 1929. Major earthquakes occurred off Shikoku in 1854 (Ansei, $M = 8+$) and 1946 (Nankaido, $M = 8.2$). For Hokkaido the observed uplift rates [*Shimazaki*, 1974*a*] are based on changes in elevation between leveling surveys in 1903 and 1955, but similar rates would be inferred from elevation changes between 1955 and 1972 [*Abe*, 1978]. Major earthquakes occurred off the Hokkaido coast in 1894 (Kushiro-Oki, $M = 7.9$) and 1973 (Nemuro-Oki, $M = 7.4$). For Tohoku the observed uplift rates [*Seno*, 1979] are based on changes in elevation between the surveys of 1894-1899 and the survey of 1942 across Tohoku at the latitude of Sendai. The predominately negative uplift rates observed during that interval apparently changed to positive uplift rates in the intervals 1942-1956, 1956-1966, and 1966-1973 [*Kato*, 1979, p. 159]. Major earthquakes occurred off the coast of Tohoku near Sendai in 1897 (Sendai-Oki, $M = 7.7$), 1936 (Kinkazan-Oki, $M = 7.7$), and 1978 (Miyagi-Oki, $M = 7.4$). The uplift rates for Tohoku shown in Figure 12 may contain some coseismic effects from the 1897 and 1936 earthquakes, which could account for the discrepancies between the uplift rates for the 1894/1899-1942 epoch and the three epochs subsequent to 1942. However, the usual estimates of the magnitude of coseismic elevation changes on land in Tohoku would suggest that these effects would not modify the estimated uplift rates substan-

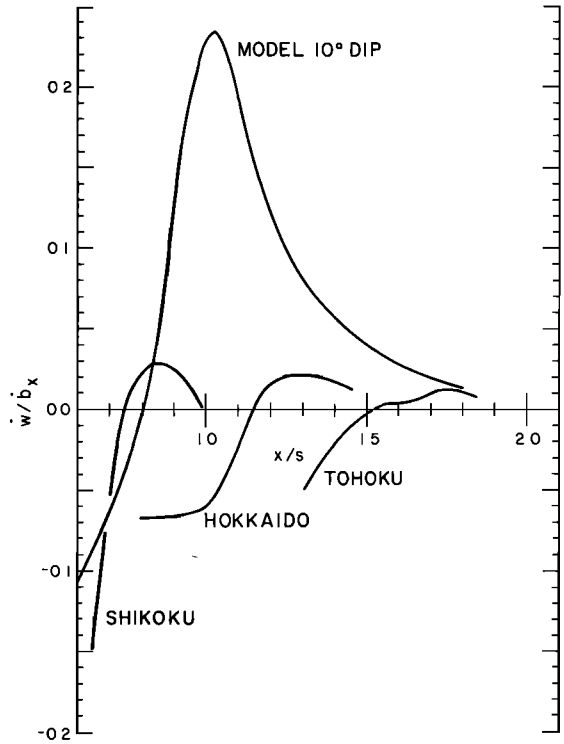

Fig. 12. Comparison of uplift rates (w) observed along the coast of Japan with the uplift rate predicted by the model shown in Figure 2; b_x is the perpendicular convergence rate of the interacting plates, and s is the downdip width of the main thrust zone. The uplift rates for Shikoku are taken from *Thatcher and Rundle* [1979], for Hokkaido from *Shimazaki* [1974*a*], and for Tohoku from *Seno* [1979].

tially [*Seno*, 1979, p. 46; *Kato*, 1979, p. 159]. Nevertheless, the observed elevation change for Tohoku shown in Figure 12 should be used with some caution. It may not be typical of the strain accumulation interval.

A comparison of the horizontal strain rates observed in Shikoku, Tohoku, and Hokkaido with rates predicted by the model of Figure 2 is shown in Table 1. The observed strain rates are deduced from angle changes accumulated over several decades as measured by triangulation surveys. The precision of the surveys is not adequate to obtain the strain locally but rather the strain must be averaged over broad areas (eastern half of Shikoku, the breadth of Tohoku, and the width of eastern Hokkaido). The observed strains attributed to *Nakane* [1973] in Table 1 refer to the total engineering shear strain (i.e., twice the tensor shear strain), whereas those attributed to *Seno* [1979] and *Shimazaki* [1974*a*] refer to horizontal extension in the direction of plate convergence (e_{xx} in Figure 2). Where the plate motion is perpendicular to the trench axis (Shikoku and Tohoku), the two measures of strain should be identical, but where oblique convergence obtains (Hokkaido), the transverse component of plate motion will contribute to the shear strain. However, the contribution of transverse shear to the strains in Table 1 is quite small, and the predicted strain rates in that table may be read either as perpendicular extension or total shear. In general, the strain estimates from *Nakane* [1973] in Table 1 are preferred because shear strain is free from the systematic bias associated with scale, which contaminates measures of extension deduced from triangulation.

It is clear from Figure 12 that the predicted uplift profile does not fit the observed uplift profiles. The agreement is worst for the Tohoku profile where the trend is almost exactly opposite to the predicted trend. However, the Tohoku data may be contaminated by coseismic effects from the 1897 and 1936 earthquakes, in which case the profile predicted from the strain accumulation period need not be comparable. The Hokkaido profile shows substantial subsidence where uplift is predicted. The Shikoku profile does bear some resemblance to the predicted profile, but it is systematically biased toward more negative uplift rates. No minor modifications of the model parameters would be adequate to bring the predicted uplift profile in Figure 12 into reasonable agreement with any of the observed profiles.

TABLE 1. Comparisons of Strain Rates Observed in Japan With the Interseismic Strain Rates Predicted From the Dislocation Model of Figure 2

	Observed Strain Rate			
Location	Time Interval	Source	Rate, μstrain/yr	Predicted Strain Rate, μstrain/yr
Shikoku	1948-1971	Nakane [1973]	-0.26	-0.07
Tohoku	1893/1904-1962	Nakane [1973]	-0.13	-0.1
	1893/1904-1962	Seno [1979]	-0.06	-0.1
Hokkaido	1903/1908-1967	Nakane [1973]	-0.17	-0.08
	1903/1908-1967	Shimazaki [1974a]	-0.05	-0.08

The effects of asthenosphere flow and buoyancy on the model solution in Figure 12 can be inferred from *Rundle*'s [1982, Figure 4] analysis of thrust faulting in an elastic-viscoelastic earth model with the effects of gravity included. Rundle showed that the transient viscoelastic response dies out much more rapidly in the presence of gravity, and consequently, his solution for large t approximates the solution for an elastic plate over a perfect fluid. Rundle's solution for a 30°-dipping normal fault is shown in Figure 13. In that figure the solid lines represent coseismic response, the dashed line represents the additional viscoelastic-buoyant response, and the dotted line represents the total response (sum of the dashed and solid curves). That is, the solid and dotted curves in Figure 13 represent the function $-w_1(x,\infty)$ for the elastic half space and the elastic plate overlying a fluid substrate, respectively. Inasmuch as the uplift rate is simply $-w_1(x,\infty)/T$, where T is the earthquake interoccurrence time (see equation 9), the more exact solution introduces an even greater discrepancy between the predicted and observed uplift rates in Figure 12 (i.e., the uplift near $x/s = 0$, already much too large in the figure, would be increased substantially).

The differences between the observed profiles in Figure 12 are perhaps as significant as the discrepancies between the predicted and observed profiles. The uplift profiles in Figure 12 are scaled according to the postulated characteristic dimensions of the problem (i.e., distance in units of the width of the main thrust zone and uplift rate in units of the convergence rate), and one might expect those profiles to be identical in such a plot. The range of uplift and convergence rates for the data in Figure 12 is insufficient to judge the success of the scaling relation for uplift rates, but a significant change in the horizontal scaling factors (190, 290, and 370 km for Shikoku, Hokkaido, and Tohoku, respectively, rather than 200 km as used for all three profiles in Figure 12) is needed to bring the three observed profiles into approximate coincidence.

The strain observations show a rough correspondence to the predicted strain rates (Table 1), although the significance of this agreement is questionable in view of the lack of agreement between uplift profiles (Figure 12). The worst agreement is for the strain rates at Shikoku, where the observed strain rate is almost 4 times larger than the predicted rate. The observation period 1948-1972 at Shikoku follows rather closely after the 1946 earthquake, and the higher observed rate might be related to immediate postearthquake readjustment not accounted for in the simple elastic model. The observed strain rates at Tohoku and Hokkaido agree with the predicted rates within a factor of about 2.

Obviously, the uplift profile predicted by the dislocation model using an elastic half-space model fails to explain the uplift profile observed in Japan. It is quite possible that this failure is due to the extremely simple elastic half-space earth model employed. However, we have shown (Figure 13) that the more appropriate elastic model, an elastic plate over a fluid substrate, leads to an even greater discrepancy between predicted and observed deformation. Perhaps, the time-dependent effects in the elastic-viscoelastic earth models can account for the observed deformation along the coast of Japan, but the linear-in-time deformation observed (Figure 11) suggests that this is not the case. Such elastic-viscoelastic models are being investigated more closely by *Thatcher and Rundle* [1981; manuscript in preparation, 1983]. It is perhaps more likely that the trouble is not in the earth model employed but rather in the dislocation model itself. For example, how realistic is it to assume that the entire main thrust zone is

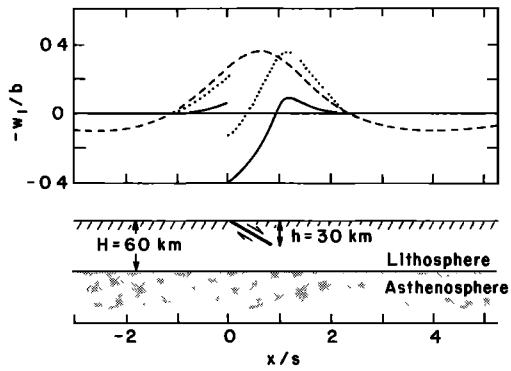

Fig. 13. Surface uplift ($-w_1$) produced by normal slip b on a two-dimensional dip slip fault dipping 30° from the surface to a depth h = 30 km in a 60-km-thick elastic plate overlying a viscoelastic (Maxwell solid) substrate (model illustrated in lower sketch). The downdip width of the fault is s = 60 km. In the upper figure the solid curve represents the coseismic surface uplift, the dashed curve represents the additional uplift due to viscoelastic relaxation and buoyancy in the period of 45 asthenosphere relaxation times (relaxation is virtually complete at that time), and the dotted curve represents the sum of the other two [from *Rundle*, 1982, Figure 4].

locked in the interseismic period. Perhaps only isolated patches of the main thrust zone lock. Certainly, the rupture areas postulated for the major offshore Japanese earthquakes do not span the entire main thrust zone [*Kawakatou and Seno*, 1983].

As has been shown earlier by *Shimazaki* [1974a], *Seno* [1979], and *Kato* [1979], surface uplift observed in Japan can be explained (e.g., Figure 9) using an elastic half-space earth model by postulating that stick slip extends on the plate interface to depths of perhaps 100 km or more, well beyond the main thrust zone. However, plausible physical arguments indicate that it is unreasonable to expect stick slip much beyond the lower end of the main thrust zone [*Kato*, 1979; *Seno*, 1979; *Wahr and Wyss*, 1980]. The most direct of these arguments involves the absence of interplate earthquakes on the plate interface beyond the end of the main thrust zone [*Yoshii*, 1979]. Other arguments depend upon the distinct material properties inferred for the wedge of mantle above the subducted oceanic lithosphere and below the crust of the overthrust plate. The properties of this wedge (low Q, low velocity of elastic shear waves), the absence of seismicity within it, and the high heat flow observed at the surface above it suggest that it may be a locus of partial melting, perhaps furnishing magma for the volcanic arc. It is unlikely that stick slip would occur in such an environment.

Although there is substantial doubt that stick slip on the plate interface can occur far beyond the downdip end of the main thrust zone, the consequences to the deformation cycle of such a circumstance are shown in Figure 14. If one takes s = 200 km, then stick slip would extend to a depth of about 98 km on the fault shown in that figure. If a constant slip of amount b_x occurs over the entire fault surface shown in the bottom panel of Figure 14 then the uplift is as shown at the top of the figure. The nodal (no uplift) line occurs at 290 km from the trench. As the slip is decreased on the lower portion of the fault, the nodal line shifts toward the trench (second, third, and fourth diagrams in Figure 14). Crude approximations to the uplift profiles observed at Tohoku, Hokkaido, and Shikoku are given by the first, third, and fourth plots, respectively, in Figure 14. However, such fits cannot be very convincing in view of the arguments against stick slip along

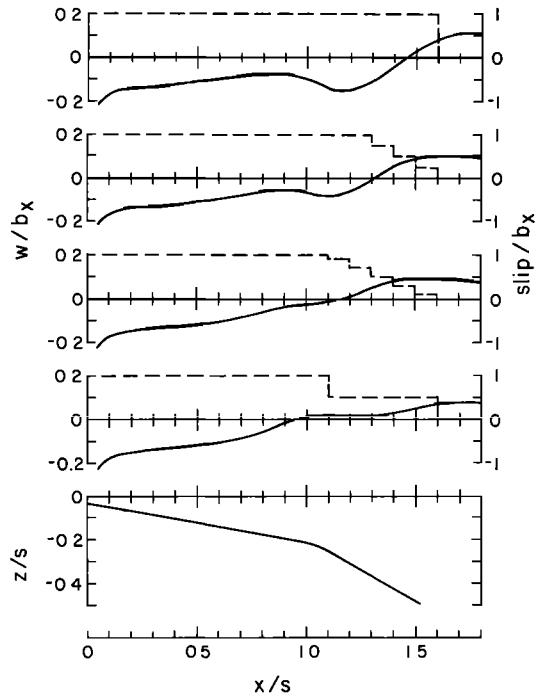

Fig. 14. Uplift as a function of distance from the trench for four different distributions of slip on the fault model shown in the bottom diagram. In each of the upper four diagrams the solid line represents the uplift and the dashed line the distribution of slip on the fault; s is the width of the main thrust zone (segment of fault above the bend). For the dashed line the abscissa is not x/s, but rather the distance downdip along the fault in units of s and the ordinate is slip/b_x (right scale).

the plate interface at depth and also the large lithosphere thickness (>100 km) required by the model.

Finally, the discrepancy between the predicted and observed uplift profiles in Figure 11 may be due to a rapid secular subsidence along the coast of Japan, perhaps due to detachment of the subducted plate [*Abe*, 1977, p. 286; *Kato*, 1979, p. 163]. This would, of course, contradict the assumption in the dislocation model that steady state subduction is free from secular deformation. There is no particular evidence for secular uplift or subsidence at Shikoku (the uplifted coastal terraces there are apparently associated with local imbricate faulting [*Fukao*, 1979, p. 2313]), but arguments exist for secular subsidence at both Tohoku and Hokkaido. On Hokkaido the Hanasaki tide gage record [*Abe*, 1978, p. 267] shows that subsidence has continued at a rate of about 9 mm/a since about 1910 with no appreciable recovery at the time of the 1973 earthquake. Either the 1973 earthquake was not the major thrust event that terminates an earthquake cycle, or the 9 mm/a subsidence rate represents secular subsidence not earthquake recovery. A long-term (5000 a) geologic measure of secular subsidence in southeastern Hokkaido suggests a much lower (0.4 mm/a) subsidence rate [*Abe*, 1978]. For Tohoku, *Shimazaki* [1974b, p. 324] and *Kato* [1979, p. 165] cite a locally deformed, submerged, wave-cut cliff as evidence for long-term subsidence (perhaps 4 mm/a for 0.05 Ma), but *Seno* [1979, p. 44] argues that marine terraces indicate approximate stability or even minor uplift over the past 0.14 Ma. Thus evidence for appreciable secular subsidence along the coast of northern Japan is at best equivocal.

Kasahara and Kato [1981] have proposed a compound deformation cycle to explain the secular subsidence observed along the Pacific coast of Tohoku and Hokkaido. In their model the two plates at the subduction zone are tightly coupled to a depth of about 100 km. The main thrust zone ruptures on the order of about once every 100 a. A very minor partial decoupling of the uppermost part of the Benioff interface by aseismic creep may follow each seismic event; but, in general, stress across the upper Benioff interface above 100 km depth accumulatives with time. Ultimately, the stress becomes sufficiently high that the next abrupt failure of the main thrust zone loads the upper Benioff interface beyond its strength and causes major aseismic creep along that interface. Because coastal subsidence may be caused by the absence of slip on the upper Benioff interface at Tohoku and Hokkaido, the subsidence cycle would then extend over several earthquake cycles, and on a time scale of one or two earthquake cycles there would appear to be a secular subsidence of the coast. But that subsidence itself would be cyclic, being recovered completely following some subsequent earthquake.

CONCLUSIONS

A plausible model of the earthquake cycle at a subduction zone is based on the proposal that relative plate motion is accommodated by stick slip on the main thrust zone and by aseismic slip elsewhere on the plate interface. The deformation produced at the free surface of the overthrust plate by that process is completely equivalent to the deformation produced by repeated cycles of slip on the main thrust zone, each cycle consisting of a long interval of backward (i.e., opposite in sense to that implied by the relative plate movement) slip at the rate of relative plate motion terminated by abrupt forward slip of the amount needed to recover the accumulated backward slip. This slip cycle on the main thrust zone is a simple dislocation process for which standard solutions are available. In an elastic earth model the deformation cycle consists of an abrupt coseismic offset followed by a linear-in-time recovery in the remainder of the interseismic interval. In a model involving viscoelastic elements (e.g., elastic plate over a viscoelastic half space) the deformation cycle consists of an abrupt coseismic offset followed by a nonlinear-in-time recovery. In general, records of interseismic deformation indicate relatively linear long-term recovery, suggesting that the overall process can be described adequately by an elastic earth model, although the explanation of some details may require viscoelastic elements. Finally, comparison of the deformation predicted along the coast of Japan with that observed there is unsatisfactory as long as stick slip is confined to the main thrust zone. Satisfactory agreement can be obtained if stick slip on the plate interface is extended to a depth of near 100 km, well beyond the down- dip end of the main thrust zone (depth 40 km). The dislocation model readily accommodates this extension of the domain of stick slip. However, seismicity and the inferred physical properties of the mantle wedge lying above the subducted plate indicate that stick slip is unlikely to occur much beyond the downdip edge of the main thrust zone (40-km depth). This dilemma is unresolved.

Acknowledgments. Wayne Thatcher has provided advice and criticism during the preparation of this paper, and K. Shimazaki and H. J. Melosh suggested important changes in the original manuscript.

REFERENCES

Abe, K., Tectonic implications of the large Shioya-Oki earthquakes of 1938, *Tectonophysics, 41*, 269-289, 1977.

Abe, K., Some problems in the prediction of the Nemuro-Oki earthquake, in *Earthquake Precursors*, edited by C. Kisslinger and Z. Suzuki, pp. 261-271, Japan Scientific Societies Press, Tokyo, 1978.

Davies, J. N., and L. House, Aleutian subduction zone seismicity, volcano-trench separation, and their relation to great thrust-type earthquakes, *J. Geophys. Res.*, *84*, 4583-4591, 1979.

Freund, L. B., and D. M. Barnett, A two-dimensional analysis of surface deformation due to dip-slip faulting, *Bull. Seismol. Soc. Am.*, *66*, 667-675, 1976.

Fukao, Y., Tsunami earthquakes and subduction processes near deep-sea trenches, *J. Geophys. Res.*, *84*, 2303-2314, 1979.

Hirahara, K., Three-dimensional seismic structure beneath southwest Japan: The subducting Philippine sea plate, *Tectonophysics*, *79*, 1-44, 1981.

Kasahara, K., Aseismic faulting following the 1973 Nemuro-Oki earthquake, Hokkaido, Japan (a possibility), *Pure Appl. Geophys.*, *113*, 127-139, 1975.

Kasahara, K., and T. Kato, Aseismic faulting following the 1973 Nemura-Oki earthquake, Hokkaido, Japan (a retrospective study), *Pure Appl. Geophys.*, *119*, 392-403, 1981.

Kato, T., Crustal movements in the Tohoku district, Japan, during the period 1900-1975, and their tectonic implications, *Tectonophysics*, *60*, 141-167, 1979.

Kawakatsu, H., and T. Seno, Triple seismic zone and the regional variation of seismicity along the northern Honshu arc, *J. Geophys. Res.*, in press, 1983.

Matsu'ura, M., T. Tanimoto, and T. Iwasaki, Quasi-static displacements due to faulting in a layered half-space with an intervenient viscoelastic layer, *J. Phys. Earth*, *29*, 23-54, 1981.

Moss, W. C., and W. G. Hoover, Edge dislocation displacement in an elastic strip, *J. Appl. Phys.*, *49*, 5449-5451, 1978.

Mura, T., The continuum theory of dislocations, *Adv. Mater. Res.*, *3*, 1-108, 1968.

Nakane, K., Horizontal tectonic strain in Japan, II (in Japanese), *J. Geod. Soc. Jpn.*, *19*, 200-208, 1973.

Nur, A., and G. Mavko, Postseismic viscoelastic rebound, *Science*, *183*, 204-206, 1974.

Rundle, J. B., Viscoelastic crustal deformation by finite quasi-static sources, *J. Geophys. Res.*, *83*, 5937-5945, 1978.

Rundle, J. B., Viscoelastic-gravitational deformation by a rectangular thrust fault in a layered earth, *J. Geophys. Res.*, *87*, 7787-7796, 1982.

Savage, J. C., and R. O. Burford, Geodetic determination of relative plate motion in central California, *J. Geophys. Res.*, *78*, 832-845, 1973.

Savage, J. C., and W. H. Prescott, Asthenosphere readjustment and the earthquake cycle, *J. Geophys. Res.*, *83*, 3369-3376, 1978.

Scholz, C. H., and T. Kato, The behavior of a convergent plate boundary: Crustal deformation in the south Kanto district, Japan, *J. Geophys. Res.*, *83*, 783-797, 1978.

Seno, T., Instantaneous rotation vector of Philippine Sea plate relative to the Eurasian plate, *Tectonophysics*, *42*, 209-226, 1977.

Seno, T., Intraplate seismicity in Tohoku and Hokkaido and large interplate earthquakes: A possibility of a large interplate earthquake off the southern Sanriku coast, northern Japan, *J. Phys. Earth*, *27*, 21-51, 1979.

Shimazaki, K., Preseismic crustal deformation caused by an underthrusting oceanic plate, in eastern Hokkaido, Japan, *Phys. Earth Planet. Inter.*, *8*, 148-157, 1974*a*.

Shimazaki, K., Nemuro-Oki earthquake of June 17, 1973: A lithospheric rebound at the upper half of the interface, *Phys. Earth Planet. Inter.*, *9*, 314-327, 1974*b*.

Spence, D. A., and D. L. Turcotte, Viscoelastic relaxation of cyclic displacements on the San Andreas fault, *Proc. R. Soc. London, Ser. A*, *365*, 121-144, 1979.

Thatcher, W., and J. B. Rundle, A model for the earthquake cycle in underthrust zones, *J. Geophys. Res.*, *84*, 5540-5556, 1979.

Thatcher, W., and J. B. Rundle, A viscoelastic model for periodically recurring earthquakes in subduction zones (abstract), *Eos Trans AGU*, *62*, 1031, 1981.

Thatcher, W., T. Matsuda, T. Kato, and J.B. Rundle, Lithosphere loading by the 1896 Riku-u earthquake, northern Japan: Implications for plate flexure and asthenospheric rheology, *J. Geophys. Res.*, *85*, 6429-6435, 1980.

Turcotte, D. L., and D. A. Spence, An analysis of strain accumulation of a strike slip fault, *J. Geophys. Res.*, *79*, 4407-4412, 1974.

Wahr, J., and M. Wyss, Interpretation of postseismic deformation with a viscoelastic relaxation model, *J. Geophys. Res.*, *85*, 6471-6477, 1980.

Yamashina, K., Drag model and crustal deformation in the Japanese islands (in Japanese), *Program Abstr. Seismol. Soc. Jpn.*, *1*, 56, 1976.

Yoshii, T., A detailed cross-section of the deep seismic zone beneath northeastern Honshu, Japan, *Tectonophysics*, *55*, 349-360, 1979.

(Received March 31, 1982;
revised February 22, 1983;
accepted February 23, 1982.)